Morphological instability at topological defects in a three-dimensional vertex model for spherical epithelia

Oliver M. Drozdowski and Ulrich S. Schwarz*

Institute for Theoretical Physics and BioQuant, Heidelberg University, 69120 Heidelberg, Germany

(Dated: March 15, 2024)

Epithelial monolayers are a central building block of complex organisms. Topological defects have emerged as important elements for single cell behavior in flat epithelia. Here we theoretically study such defects in a three-dimensional vertex model for spherical epithelia like cysts or intestinal organoids. We find that they lead to the same generic morphological instability to an icosahedral shape as it is known from spherical elastic shells like virus capsids, polymerized vesicles or buckyballs. We derive analytical expressions for the effective stretching and bending moduli as a function of the parameters of the vertex model, in excellent agreement with computer simulations. These equations accurately predict both the buckling of a flat epithelial monolayer under uniaxial compression and the faceting transition around the topological defects in spherical epithelia. We further show that localized apico-basal tension asymmetries allow them to reduce the transition threshold to small system sizes.

Introduction. Epithelial monolayers are a central element of the architecture of complex organisms. They separate different compartments, can form highly convoluted shapes and have exceptional mechanical properties. In particular, they can quickly undergo transitions between fluid-like and elastic properties [1, 2], driven e.g. by cell density or the aspect ratios of single cells. In general, the properties of the single cells are essential to understand the physical properties of epithelial monolayers. Topological defects defined by the neighborhood relations of the single cells have emerged as especially important elements for transformations in epithelial monolayers [3]. For example, it has been found that single cells tend to be extruded at such topological defects [4]. While topological defects are a natural ingredient of hydrodynamic theories [5], it is challenging to include them in elastic descriptions of monolayers [6–8].

Here we show that spherical epithelia like cysts or intestinal organoids are a natural starting point to study the global effects of topological defects in epithelial monolayers. They are experimentally very accessible and of large biomedical relevance [9]. Due to Euler's polyhedron theorem, they necessarily have to include twelve pentagons in the close-packed tiling of the spherical surface [10]. In order to combine these topological defects with the typical mechanical properties of epithelial monolayers, we employ a three-dimensional (3D) vertex model (VM), in which cells are described as polyhedra with a fixed volume and with polygonal faces contributing to the total energy through surface tensions [11]. The 3D VM has been used before for modeling spherical epithelia [6, 12–15], but coarse-graining procedures have not been able to fully address the role of topological defects in such a setting.

By simulating the 3D VM for complete spherical epithelial shells, we discovered an icosahedral faceting instability. While small shells with few cells have a spherical shape (Fig. 1(a)), larger icosahedral shells experience
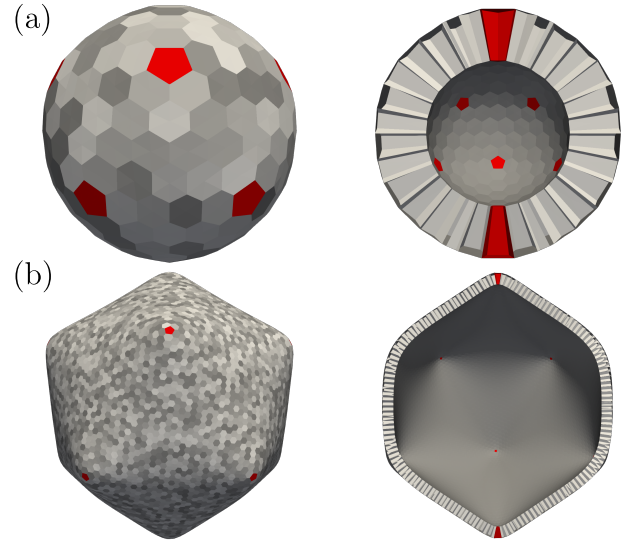

FIG. 1. Spherical epithelia described by a 3D vertex model experience an icosahedral instability that is well known for spherical elastic shells like virus capsids, polymerized vesicles or buckyballs. (a) A small epithelial shell stays spherical. (b) A large epithelial shell becomes faceted with icosahedral symmetry. Cells are arbitrarily colored in grey and pentagonal cells, which are topological defects, are shown in red.

conical instabilities at the pentagonal defects (Fig. 1(b)) [16]. This transition is well known for two-dimensional elastic crystals [10, 17], including virus capsids [10, 18], polymerized vesicles [19, 20], and buckyballs [21], but has not been described before for spherical epithelia. Our numerical results suggest that a continuum limit exists for the 3D VM that like thin elastic shells contains both stretching and bending energies. Here we show how such a coarse-graining procedure can be performed and that it explains the morphological instability. We further show that the threshold for this instability can be actively controlled by epithelia through apico-basal polarity.

Continuum model. We start with the Hamiltonian of a 3D VM with apical, basal and lateral faces,

$$E_{\mathrm{VM}} = \sum_{\mathrm{cells}} \left(\Gamma_{\mathrm{a}} A_{\mathrm{a}} + \Gamma_{\mathrm{b}} A_{\mathrm{b}} + \frac{1}{2} \sum_{\mathrm{lateral\ faces}} \Gamma_{\mathrm{l}} A_{\mathrm{l}} \right), \quad (1)$$

with surface tensions Γ_i and areas A_i for apical, basal and lateral faces, respectively ($i = $ a, b, l). The factor $1/2$ avoids membrane double counting. Assuming volume V being conserved, we non-dimensionalize energy with Γ_{l} and length with $V^{1/3}$.

To derive a thin-plate theory from the 3D VM, we consider the nonlinear theory of moderately bent plates, where the total energy is given by stretching and bending energy contributions [22]. For the in-plane stretching energy we assume the usual energy density

$$e_{\mathrm{stretch}} = \frac{1}{2} \left(2\mu \varepsilon_{ij}^2 + \lambda \varepsilon_{kk}^2 \right), \quad (2)$$

with two-dimensional strain tensor $\boldsymbol{\varepsilon}$ and Lamé coefficients μ and λ. We determine the Lamé coefficients in a flat configuration in a mean-field fashion, following ideas from earlier work on 2D VMs [23–25]. We consider a constant strain tensor for an individual cell, i.e. we assume strain to vary on a larger length scale than cell size. We assume a regular n-gonal lattice structure, which we will take to be a hexagonal lattice with $n = 6$. We then determine the energy density for a given strain. The equilibrium height can be obtained via minimization of Eq. (1) at constant volume. For the lateral faces we employ an angular averaging method (described in detail in the supplement [26]). In addition we consider non-affine deformations, as previously described for 2D models [25, 27]. Non-affine relaxations correspond to additional relative deformations of the two sublattices that make up the hexagonal lattice and can be included by allowing for an additional degree of freedom in the mid-plane shape, which allows for force balance at triple membrane junctions via angular relaxation. Note that the $\pi/3$ rotational symmetry implies that our 2D continuum model has only two elastic constants, exactly like an isotropic 2D material.

Considering the deformed areas and Taylor-expanding in the principal strains, we find $2\mu = \lambda = \Gamma_{\mathrm{a}} + \Gamma_{\mathrm{b}}$, or, equivalently,

$$Y = \frac{4\mu(\mu + \lambda)}{2\mu + \lambda} = \frac{3}{2}(\Gamma_{\mathrm{a}} + \Gamma_{\mathrm{b}}), \quad \nu = \frac{\lambda}{2\mu + \lambda} = \frac{1}{2}, \quad (3)$$

for the two-dimensional Young's modulus and Poisson ratio, respectively. The Young's modulus does not depend on the lateral tension Γ_{l}, because both $\Gamma_{\mathrm{a/b}}$ and Y are in units of Γ_{l}. The reason is that changes in Γ_{l} will affect height and edge length in such a manner that the energy density stays the same. A 2D Poisson ratio of $1/2$ means that the sheet is compressible (incompressible materials in 2D have $\nu = 1$), because it can

exchange material between the in-plane and out-of-plane dimensions. In addition, we formulated the stretching energy in the fully nonlinear setting (see supplement [26]). The resulting energy density does not match standard hyperelastic models [28]. Thus in the following we restrict ourselves to the first (cubic) correction to the linear theory as obtained by a Taylor expansion. This yields $Y_{\mathrm{nl}} = \left(\frac{3}{2} - \frac{7}{4}\varepsilon_{xx} \right)(\Gamma_{\mathrm{a}} + \Gamma_{\mathrm{b}})$ and $B_{\mathrm{nl}} = \left(\frac{3}{2} - \varepsilon_{xx} \right)(\Gamma_{\mathrm{a}} + \Gamma_{\mathrm{b}})$ for the Young's modulus and bulk modulus in uniaxial and isotropic stretching, respectively.

For the bending energy density we assume the Helfrich form

$$e_{\mathrm{bending}} = \frac{\kappa}{2}(H - c_0)^2 + \kappa_{\mathrm{G}} K, \quad (4)$$

with bending rigidity κ, mean total curvature $H = c + c'$ with the principal curvatures c and c', spontaneous curvature c_0, saddle splay modulus κ_{G} and Gauss curvature $K = cc'$. Rozman et al. [12] have proposed a method to determine these quantities for the 3D VM using quadratic lattices. We generalized this to hexagonal lattices and adapted it such that we can formulate a theory for moderate bending.

Consider a cell which is bent with principal curvatures c and c' and with unchanged center height. Volume conservation and curvatures determine the apical, basal and lateral face areas after deformation. Normalizing to the undeformed mid-plane area (for consistency and different from Ref. [12]) and Taylor-expanding with respect to ch and $c'h$ yields the bending energy density (see supplement for full derivation [26]). Like for the stretching part, we also consider non-affine deformations, which leads to a correction factor k_c. For $n = 6$ we find

$$\kappa = \frac{9}{8} \frac{k_c}{2^{1/3} 3^{4/3}} (\Gamma_{\mathrm{a}} + \Gamma_{\mathrm{b}})^{1/3},$$

$$\kappa_{\mathrm{G}} = \left[\frac{(\Gamma_{\mathrm{a}} + \Gamma_{\mathrm{b}})^2}{2} + \frac{3}{2} - \frac{9}{4}k_c \right] \frac{(\Gamma_{\mathrm{a}} + \Gamma_{\mathrm{b}})^{1/3}}{2^{1/3} 3^{4/3}}, \quad (5)$$

$$c_0 = \frac{4}{3} 2^{2/3} 3^{1/6} (\Gamma_{\mathrm{a}} + \Gamma_{\mathrm{b}})^{1/3} (\Gamma_{\mathrm{b}} - \Gamma_{\mathrm{a}}).$$

Bending with $c \neq c'$ is accompanied by non-isotropic stretching in the apical and basal planes and angular relaxation, similarly as in non-isotropic stretching of the mid-plane. For $c = c'$ such non-affine relaxations do not occur since lateral membrane angles do not change. In this case the energy is identical to the case of $k_c = 1$, but otherwise k_{c} is a numerical factor that we obtain from fitting to the simulation results for cylindrical surfaces.

The results from Eq. (5) differ in several essential ways from the known formulae for thin elastic plates. For a thin elastic plate the bending rigidity would scale like $\kappa \propto Yh^2$ (with 2D Young's modulus $Y = Y_{\mathrm{3D}}h$). With our result for Y and the reference height $h \propto (\Gamma_{\mathrm{a}} + \Gamma_{\mathrm{b}})^{2/3}$ (compare supplement [26]), this would lead to $\kappa \propto (\Gamma_{\mathrm{a}} + \Gamma_{\mathrm{b}})^{7/3}$. As seen in Eq. (5), the bending rigidity depends more weakly on the tensions, because
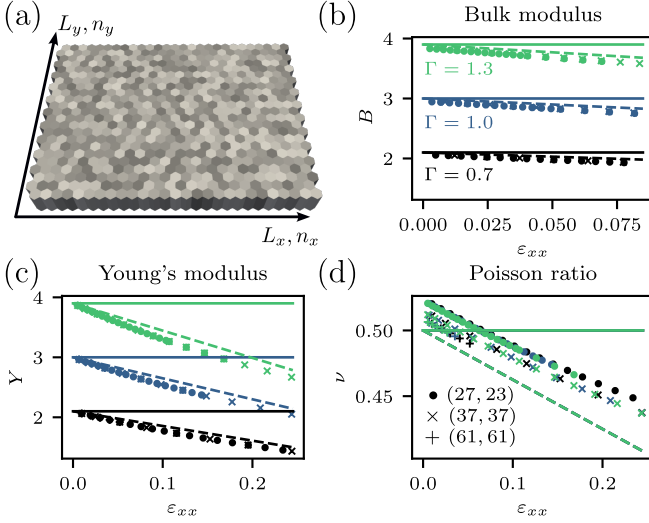
FIG. 2. Stretching of a rectangular 3D VM monolayer. (a) Depiction of the simulated monolayer with arbitrary coloring of individual cells. (b) Bulk modulus B for isotropic stretching with strain ε_{xx}. (c,d) Young's modulus Y and Poisson ratio ν for uniaxial stretching with strain ε_{xx}. Colors indicate different surface tensions Γ and symbols different plate sizes (n_x, n_y). Dashed and solid lines are the predictions from nonlinear and linear continuum theories, respectively.

FIG. 3. Bending of a rectangular 3D VM monolayer. (a) Bending rigidity κ as determined from a cylindrically bent monolayer. (b) Saddle splay modulus κ_{G} as determined from a spherically bent monolayer.

we do not have to consider the area changes along the entire height. In fact, compression on one of the sides will lower the energy instead of increasing it, as it is the case in 3D elastic plates. The dependence is much stronger, however, for the saddle-splay modulus, as we cannot compensate for area changes of the polygonal faces via shape changes (e.g. from rectangles to trapezoids) when both curvatures do not vanish. We have the same leading order scaling as we would have for elastic plates because here the apical and basal area changes for a given curvature also enter quadratically in the cell height. The spontaneous curvature depends on the apico-basal tension asymmetry, as this introduces a preferred curvature to minimize the energies. For $\Gamma_{\mathrm{a}} = \Gamma_{\mathrm{b}}$ it vanishes as expected.

Like for a thin plate, the full deformation energy can now be calculated as

$$E = \int (e_{\mathrm{stretch}} + e_{\mathrm{bending}})\, \mathrm{d}S. \qquad (6)$$

For moderately bent plates there is an additional coupling between the two terms. A mid-plane deflection $f(x,y)$ will contribute to the strain tensor as $\varepsilon_{ij} = (\partial_i u_j + \partial_j u_i + \partial_i f \partial_j f)/2$, with deformation u_i in i-direction.

Stretching and bending of a flat sheet. To test the continuum theory by computer simulations, we have implemented the 3D VM, Eq. (1), as module in the software suite Chaste [29], similarly to Ref. [11] (details in the supplement [26]). For stretching we implemented a finite-
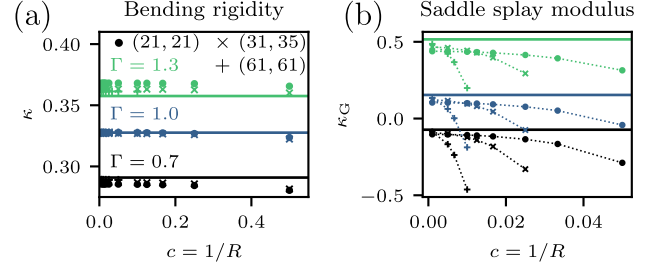
size rectangular plate of hexagonal cells. The monolayer consists of n_x and n_y cells in the x and y-directions, respectively (Fig. 2(a)). For now we assume $\Gamma_{\mathrm{a}} = \Gamma_{\mathrm{b}} = \Gamma$, i.e. we do not consider a spontaneous curvature c_0 from apico-basal polarity.

First we considered isotropic stretching with edge stresses $\sigma_{xx} = \sigma_{yy}$ and measured the effective bulk modulus as $B = \lambda + \mu = \varepsilon_{xx}/2\sigma_{xx}$. Then we considered uniaxial stretching with edge stresses $\sigma_{yy} = 0$ and measured Young's modulus as $Y = \sigma_{xx}/\varepsilon_{xx}$ and Poisson ratio as $\nu = -\varepsilon_{yy}/\varepsilon_{xx}$. Fig. 2(b-c) demonstrates excellent agreement between the simulations results (symbols) and the nonlinear continuum theory (dashed lines). Moreover the elastic moduli B and Y from Eq. (3) (solid lines) correspond exactly to the limiting cases of vanishing strain. The Poisson ratio ν is close to $1/2$ as predicted by Eq. (3). In the following, we will mainly discuss the case of linear elasticity, but will come back to our nonlinear results when needed.

Next we simulated bending of cylindrical and spherical surfaces. Fig. 3(a) shows the resulting bending rigidity κ as function of curvature $c = 1/R$ of a cylinder segment with mid-plane radius R. For $\Gamma = 1$, we determine the non-affinity correction factor by a fit as $k_c \approx 1.26$ and show that it is caused by non-affine apical and basal deformations (compare supplement [26]). Our simulation results (symbols) agree well with the prediction from continuum theory, Eq. (5) (solid lines). Fig. 3(b) shows the results for the saddle splay modulus κ_{G}. For this stretching contributions, arising from the non-developable spherical deformation, were determined via finite element simulations, implemented with FEniCS [26, 30]. Again we find good agreement with the theoretical pediction from Eq. (5) (solid lines) for small curvature. The deviations at larger curvature are related to finite-size effects, including overestimation of the stretching energy for differently sized plates.

Buckling of a compressed sheet. Our continuum theory effectively describes the epithelial monolayer as a moderately bent plate. A classical application of such a theory is plate buckling upon in-plane compression, which
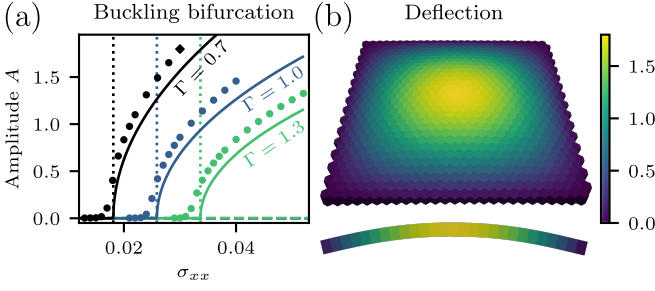
FIG. 4. Buckling instability in a simply supported 3D VM sheet of size $(27, 31)$ under uniaxial compression. (a) Buckling bifurcations in amplitude with the total compressive stress σ_{xx} as control parameter for different tensions Γ. The solid lines are the continuum mechanics results for plate buckling, the dashed line is the unstable unbuckled state, the dotted line is the critical buckling stress, and the symbols are 3D VM simulations. (b) 3D VM simulation of deflected monolayer for $\Gamma = 0.7$ and $\sigma_{xx} = 0.03$, indicated in (a) as diamond marker. Below the 3D image a cross-sectional view is shown. Color indicates the mid-plane deflection of cell.

has also been demonstrated experimentally for epithelial monolayers [31], depending on both stretching and bending.

Fig. 4(a) shows the amplitudes of a simply-supported rectangular plate, compressed along the edges parallel to the y-direction with compressive stress σ_{xx}. We assumed straight (but movable) edges, as if the plate was situated in a movable rigid frame, and found a bifurcation toward a bent state with one half-wave along both axes. The critical stress in the 3D VM is slightly smaller than the continuum expectation, which can be explained by the nonlinearities, which we have neglected in the mean-field model, and by finite-size effects of the plate. The post-buckling amplitude for straight edges can be approximated within thin-plate theory [32] and is shown with solid lines. For this the leading-order Fourier modes are considered and the energy is minimized for these modes (compare supplement [26]). We do see good agreement between this approximation and the 3D VM simulation results. In Fig. 4(b) the mid-plane deflection is shown. For large deflections we see a flattening of the profile with stronger deviations from a sinusoidal leading-order approximation, consistent with real thin elastic plates [33].

Topological defects and icosahedral instability. The elastic framework derived above for epithelial monolayers suggests to study the effect of topological defects on spherical shells in the same manner as usually done for 2D elastic crystals. In our context, the disclinations are the pentagonal cells in the hexagonal monolayer. For such a defect with disclinicity $s = 2\pi/6$, the in-plane azimuthal stretching energy of a disc scales quadratically with the radius. This deformation will become unstable toward a conical bending deformation with a logarithmic scaling in the energies for large radii [10, 17]. Thus elastic
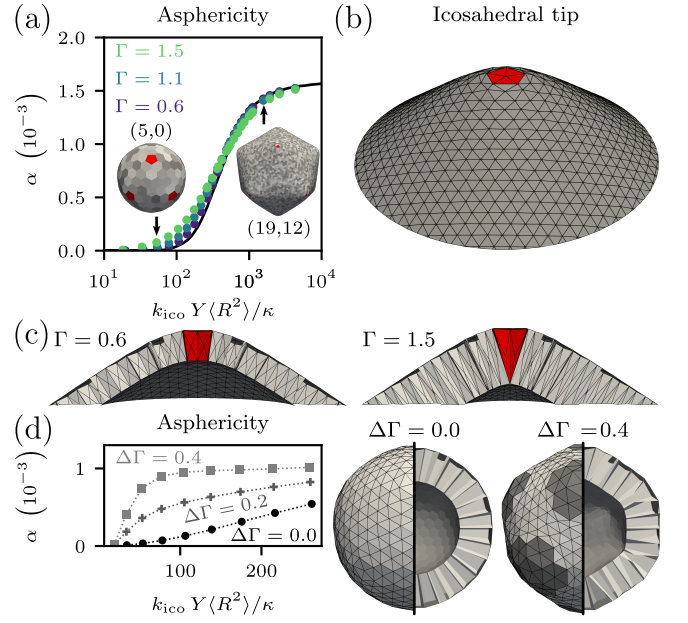

FIG. 5. Icosahedral instability of 3D VM shells. (a) Asphericity $\alpha = \langle (R - \langle R \rangle)^2 \rangle / \langle R^2 \rangle$ of the shells for different apical/basal surface tensions Γ as function of the average cell-radius. The radii are scaled by the ratio of the Young's modulus Y and bending rigidity κ with a nonlinearity correction $k_{\rm ico}$. The solid curve is the continuum prediction [10]. (b) A cut-out of the icosahedral tip for Caspar-Klug indices $(23, 0)$ [16] shows a conical deformation. (c) For large tensions the cell height increases and for large radii the inner membrane collapses at the defect. (d) Apico-basal tension asymmetry $\Delta\Gamma$ in the defects and their nearest neighbors lowers the buckling threshold. Cells with $\Delta\Gamma \neq 0$ are shaded in dark (size $(5, 0)$, $\Gamma = 1.1$).

shells of sufficient size, like large virus capsids or bucky-balls, undergo a shape instability, in which each of the 12 pentagonal defects becomes the corner of an icosahedron.

As already shown in Fig. 1, our computer simulations of the 3D VM demonstrate exactly this scenario. To provide more details, Fig. 5(a) shows the asphericity $\alpha = \langle (R - \langle R \rangle)^2 \rangle / \langle R^2 \rangle$ of the cell centers as a function of the rescaled quadratic radius. It is well known that the transition depends on the ratio of bending rigidity and Young's modulus, which sets the relevant length scale $\sqrt{\kappa/Y}$ [17]. In addition, we introduce a nonlinearity correction $k_{\rm ico}$. For an $s = 2\pi/6$ disclinicity the azimuthal strain is as large as 0.2 and we are in the strongly nonlinear regime, cf. Fig. 2(c). We find that a correction factor of $k_{\rm ico} \approx 1/2$ is necessary to account for this. With this scaling all curves in Fig. 5(a) collapse onto the continuum limit (solid line taken from the literature [10]) except for small radii. This deviation can be understood to be a finite size effect as small radii correspond to few cells and large lattice constants compared to the radius. Notice that we indeed find a conical deformation at the pentagonal tips of the icosahedron (Fig. 5(b)),

where the inner membrane can even collapse for large Γ and thus large heights (Fig. 5(c)). Experiments suggest $Y = 200$ kPa μm and $V^{1/3} \approx 10$ μm [34], resulting in $\kappa \approx 2200$ kPa μm^3 for the VM with $\Gamma = 1$. The buckling threshold is known to be $k_{\text{ico}} Y R_{\text{crit}}^2 / \kappa \approx 154$ [10]. The critical radius is thus $R_{\text{crit}} \approx 60$ μm, which is roughly the size at which intestinal organoids undergo budding [15, 35].

In passive elastic shells, topological defects tend to form additional structures such as defect scars, which screen the effect of the single defects [36, 37]. For flat epithelial monolayers it has already been established that active processes modulate their elastic behavior [11], thus also affecting the role of defects. For spherical epithelia active, apico-basally polarized forces become essential for structure formation, as observed experimentally. For example, in cell extrusion cells are pushed outward through contraction [38, 39], and in budding organoids luminal (apical) contraction in buds facilitates curvature generation [15]. To study such processes in our context, we add polarity in the pentagonal defect cells and their nearest neighbors, by using finite values for $\Delta\Gamma = \Gamma_{\text{a}} - \Gamma_{\text{b}}$. Fig. 5(d) shows that such concentration of curvature generation around the topological defects facilitates buckling at smaller radii, allowing for active control of the instability threshold. Thus the instability can already occur in a neighbourhood of a few hexagonal cells, with potential implications for organoid formation and cell extrusion in less structured epithelia. Indeed, such hexagonal regions have been observed experimentally for epithelia with and without curvature [40, 41].

In summary, here we have shown with computer simulations and analytical calculations that with growing size, spherical epithelia should undergo the same morphological instability at topological defects that is known also for elastic shells such as virus capsids. Our theory applies as long as the system is sufficiently regular and does not become too heterogeneous (e.g. by cell differentiation) before the threshold is reached. Therefore we expect that experimentally it might be observed best for highly regular epithelia, such as the retinal pigmented epithelium. Indeed, our theory might explain the formation of drusen, which are spherical or conical out-of-plane deformations in the retina linked to makular degeneration [42–44].

In the future, it has to be seen how the elastic effects described here will be modulated by the dynamics of epithelial monolayers, both on the level of single cells [45] and on the tissue level [46, 47]. At any rate, however, our theory demonstrates that topological defects are not only important for single cell behaviour, but have a strong effect on the global properties of epithelial monolayers and thus could mediate long-ranged effects.

* Corresponding author: schwarz@thphys.uni-heidelberg.de

[1] C. Pérez-González, G. Ceada, F. Greco, M. Matejčić, M. Gómez-González, N. Castro, A. Menendez, S. Kale, D. Krndija, A. G. Clark, V. R. Gannavarapu, A. Álvarez Varela, P. Roca-Cusachs, E. Batlle, D. M. Vignjevic, M. Arroyo, and X. Trepat, Mechanical compartmentalization of the intestinal organoid enables crypt folding and collective cell migration, Nat. Cell Biol. **23**, 745 (2021).

[2] N. Khalilgharibi, J. Fouchard, N. Asadipour, R. Barrientos, M. Duda, A. Bonfanti, A. Yonis, A. Harris, P. Mosaffa, Y. Fujita, A. Kabla, Y. Mao, B. Baum, J. J. Muñoz, M. Miodownik, and G. Charras, Stress relaxation in epithelial monolayers is controlled by the actomyosin cortex, Nat. Phys. **15**, 839 (2019).

[3] S. Shankar, A. Souslov, M. J. Bowick, M. C. Marchetti, and V. Vitelli, Topological active matter, Nat. Rev. Phys. **4**, 380 (2022).

[4] T. B. Saw, A. Doostmohammadi, V. Nier, L. Kocgozlu, S. Thampi, Y. Toyama, P. Marcq, C. T. Lim, J. M. Yeomans, and B. Ladoux, Topological defects in epithelia govern cell death and extrusion, Nature **544**, 212 (2017).

[5] L. A. Hoffmann, L. N. Carenza, J. Eckert, and L. Giomi, Theory of defect-mediated morphogenesis, Sci. Adv. **8**, eabk2712 (2022).

[6] E. Hannezo, J. Prost, and J.-F. Joanny, Theory of epithelial sheet morphology in three dimensions, Proc. Natl. Acad. Sci. U.S.A. **111**, 27 (2014).

[7] E. Latorre, S. Kale, L. Casares, M. Gómez-González, M. Uroz, L. Valon, R. V. Nair, E. Garreta, N. Montserrat, A. del Campo, B. Ladoux, M. Arroyo, and X. Trepat, Active superelasticity in three-dimensional epithelia of controlled shape, Nature **563**, 203 (2018).

[8] U. Andrenšek, P. Ziherl, and M. Krajnc, Wrinkling instability in unsupported epithelial sheets, Phys. Rev. Lett. **130**, 198401 (2023).

[9] H. Clevers, Modeling development and disease with organoids, Cell **165**, 1586 (2016).

[10] J. Lidmar, L. Mirny, and D. R. Nelson, Virus shapes and buckling transitions in spherical shells, Phys. Rev. E **68**, 051910 (2003).

[11] M. Krajnc, S. Dasgupta, P. Ziherl, and J. Prost, Fluidization of epithelial sheets by active cell rearrangements, Phys. Rev. E **98**, 022409 (2018).

[12] J. Rozman, M. Krajnc, and P. Ziherl, Collective cell mechanics of epithelial shells with organoid-like morphologies, Nat. Commun. **11**, 3805 (2020).

[13] M. Eiraku, N. Takata, H. Ishibashi, M. Kawada, E. Sakakura, S. Okuda, K. Sekiguchi, T. Adachi, and Y. Sasai, Self-organizing optic-cup morphogenesis in three-dimensional culture, Nature **472**, 51 (2011).

[14] S. Okuda, N. Takata, Y. Hasegawa, M. Kawada, Y. In-

oue, T. Adachi, Y. Sasai, and M. Eiraku, Strain-triggered mechanical feedback in self-organizing optic-cup morphogenesis, Sci. Adv. **4**, eaau1354 (2018).

[15] Q. Yang, S.-L. Xue, C. J. Chan, M. Rempfler, D. Vischi, F. Maurer-Gutierrez, T. Hiiragi, E. Hannezo, and P. Liberali, Cell fate coordinates mechano-osmotic forces in intestinal crypt formation, Nat. Cell Biol. **23**, 733 (2021).

[16] Here and in the following we use the Caspar-Klug classification for virus capsids to indicate shell size. The Caspar-Klug indices (h, k) describe the steps in the hexagonal lattice to go from one pentagonal cell to another with respect to lattice vectors with an opening angle of $\pi/3$. The two shells shown in Fig. 1(a) and (b) have sizes (5.0) and (19, 12), respectively.

[17] H. S. Seung and D. R. Nelson, Defects in flexible membranes with crystalline order, Phys. Rev. A **38**, 1005 (1988).

[18] T. T. Nguyen, R. F. Bruinsma, and W. M. Gelbart, Elasticity theory and shape transitions of viral shells, Phys. Rev. E **72**, 051923 (2005).

[19] A. E. Blaurock and R. C. Gamble, Small phosphatidylcholine vesicles appear to be faceted below the thermal phase transition, J. Membr. Biol. **50**, 187 (1979).

[20] L. Jia, D. Lévy, D. Durand, M. Impéror-Clerc, A. Cao, and M.-H. Li, Smectic polymer micellar aggregates with temperature-controlled morphologies, Soft Matter **7**, 7395 (2011).

[21] T. A. Witten and H. Li, Asymptotic shape of a fullerene ball, EPL **23**, 51 (1993).

[22] L. D. Landau and E. M. Lifšic, *Theory of elasticity*, 2nd ed., edited by J. B. Sykes and W. H. Reid (Pergamon Press, Oxford, 1963).

[23] D. B. Staple, R. Farhadifar, J.-C. Röper, B. Aigouy, S. Eaton, and F. Jülicher, Mechanics and remodelling of cell packings in epithelia, Eur. Phys. J. E **33**, 117 (2010).

[24] M. Moshe, M. J. Bowick, and M. C. Marchetti, Geometric frustration and solid-solid transitions in model 2d tissue, Phys. Rev. Lett. **120**, 268105 (2018).

[25] M. F. Staddon, A. Hernandez, M. J. Bowick, M. Moshe, and M. C. Marchetti, The role of non-affine deformations in the elastic behavior of the cellular vertex model, Soft Matter **19**, 3080 (2023).

[26] See Supplemental Material [URL WILL BE ADDED AFTER PUBLICATION], which includes details on the derivation of the stretching parameters (I), including a nonlinear treatment (II), and of the bending parameters (III), on the numerical implementation of the 3D VM (IV), on the finite element calculation of the stretching energy in the spherically bent epithelium (V), and on the post-buckling approximation for a compressed sheet (VI). It also includes Refs. [48, 49].

[27] N. Murisic, V. Hakim, I. G. Kevrekidis, S. Y. Shvartsman, and B. Audoly, From Discrete to Continuum Models of Three-Dimensional Deformations in Epithelial Sheets, Biophys. J. **109**, 154 (2015).

[28] P. Howell, G. Kozyreff, and J. R. Ockendon, *Applied solid mechanics*, Cambridge texts in applied mathematics (Cambridge Univ. Press, Cambridge, 2009).

[29] F. R. Cooper, R. E. Baker, M. O. Bernabeu, R. Bordas, L. Bowler, A. Bueno-Orovio, H. M. Byrne, V. Carapella, L. Cardone-Noott, J. Cooper, S. Dutta, B. D. Evans, A. G. Fletcher, J. A. Grogan, W. Guo, D. G. Harvey, M. Hendrix, D. Kay, J. Kursawe, P. K. Maini, B. McMillan, G. R. Mirams, J. M. Osborne, P. Pathmanathan, J. M. Pitt-Francis, M. Robinson, B. Rodriguez, R. J. Spiteri, and D. J. Gavaghan, Chaste: Cancer, heart and soft tissue environment, J. Open Source Softw. **5**, 1848 (2020).

[30] M. Alnæs, J. Blechta, J. Hake, A. Johansson, B. Kehlet, A. Logg, C. Richardson, J. Ring, M. E. Rognes, and G. N. Wells, The FEniCS Project Version 1.5, Arch. Numer. Softw. **3**, 9 (2015).

[31] T. P. J. Wyatt, J. Fouchard, A. Lisica, N. Khalilgharibi, B. Baum, P. Recho, A. J. Kabla, and G. T. Charras, Actomyosin controls planarity and folding of epithelia in response to compression, Nat. Mater. **19**, 109 (2020).

[32] S. P. Timoshenko and J. M. Gere, *Theory of Elastic Stability*, 2nd ed. (McGraw-Hill Book Company, New York and London, 1961).

[33] J. Rhodes, Some observations on the post-buckling behaviour of thin plates and thin-walled members, Thin-Walled Struct. **41**, 207 (2003).

[34] A. R. Harris, L. Peter, J. Bellis, B. Baum, A. J. Kabla, and G. T. Charras, Characterizing the mechanics of cultured cell monolayers, Proc. Natl. Acad. Sci. U.S.A. **109**, 16449 (2012).

[35] L. Hartl, G. Huelsz-Prince, J. van Zon, and S. J. Tans, Apical constriction is necessary for crypt formation in small intestinal organoids, Dev. Biol. **450**, 76 (2019).

[36] A. Bausch, M. J. Bowick, A. Cacciuto, A. Dinsmore, M. Hsu, D. Nelson, M. Nikolaides, A. Travesset, and D. Weitz, Grain boundary scars and spherical crystallography, Science **299**, 1716 (2003).

[37] I. García-Aguilar, P. Fonda, and L. Giomi, Dislocation screening in crystals with spherical topology, Phys. Rev. E **101**, 063005 (2020).

[38] J. Rosenblatt, M. C. Raff, and L. P. Cramer, An epithelial cell destined for apoptosis signals its neighbors to extrude it by an actin- and myosin-dependent mechanism, Curr. Biol. **11**, 1847 (2001).

[39] J. Fadul and J. Rosenblatt, The forces and fates of extruding cells, Curr. Opin. Cell Biol. **54**, 66 (2018).

[40] W. Tang, A. Das, A. F. Pegoraro, Y. L. Han, J. Huang, D. A. Roberts, H. Yang, J. J. Fredberg, D. N. Kotton, D. Bi, and M. Guo, Collective curvature sensing and fluidity in three-dimensional multicellular systems, Nat. Phys. **18**, 1371 (2022).

[41] J.-M. Armengol-Collado, L. N. Carenza, J. Eckert, D. Krommydas, and L. Giomi, Epithelia are multiscale active liquid crystals, Nat. Phys. **19**, 1773 (2023).

[42] F. Schlanitz, B. Baumann, S. Sacu, L. Baumann, M. Pircher, C. K. Hitzenberger, and U. M. Schmidt-Erfurth, Impact of drusen and drusenoid retinal pigment epithelium elevation size and structure on the integrity of the retinal pigment epithelium layer, Br. J. Ophthalmol. **103**, 227 (2019).

[43] T. Ishibashi, R. Patterson, Y. Ohnishi, H. Inomata, and S. J. Ryan, Formation of drusen in the human eye, Am. J. Ophthalmol. **101**, 342 (1986).

[44] H. Usui, A. Nishiwaki, L. Landiev, J. Kacza, W. Eichler, R. Wako, A. Kato, N. Takase, S. Kuwayama, K. Ohashi, Y. Yafai, A. Bringmann, A. Kubota, Y. Ogura, J. Seeger, P. Wiedemann, and T. Yasukawa, In vitro drusen model – three-dimensional spheroid culture of retinal pigment epithelial cells, J. Cell Sci. **132**, jcs215798 (2018).

[45] A. Janshoff, Viscoelastic properties of epithelial cells, Biochem. Soc. Trans. **49**, 2687 (2021).

[46] D. Bi, J. H. Lopez, J. M. Schwarz, and M. L. Manning, A

density-independent rigidity transition in biological tissues, Nat. Phys. **11**, 1074 (2015).

[47] A. Hernandez, M. F. Staddon, M. J. Bowick, M. C. Marchetti, and M. Moshe, Anomalous elasticity of a cellular tissue vertex model, Phys. Rev. E **105**, 064611 (2022).

[48] S. Hert and S. Schirra, 3D convex hulls, in *CGAL User and Reference Manual* (CGAL Editorial Board, 2023).

[49] K. A. Brakke, The surface evolver, Exp. Math. **1**, 141 (1992).